WEP Warwick Evans Publishing

International Journal of Mechanical and Electrical Engineering

ISSN: 3005-9615 (Print), ISSN: 3005-7132 (Online) | Volume 8, Number 1, Year 2026
DOI: https://doi.org/10.62051/ijmee.v8n1.17
Journal homepage: https://wepub.org/index.php/IJMEE/index

Full-speed Range Sensorless Control of BLDC Motor Based on HFI-SMO Composite Observation

Shengjie Zhang *, Feng Miao, Bo Cao

School of Electronic Information, Southwest Minzu University, Chengdu, Sichuan, China
* Corresponding Author: Shengjie Zhang

ABSTRACT

Brushless Direct Current (BLDC) motors are widely utilized in industrial automation, intelligent robotics, military, new energy vehicles, consumer electronics, and aerospace due to their high efficiency and reliability. To meet the demand for sensorless control across the full-speed range, this paper investigates and implements a composite rotor position observation method based on High-Frequency Injection (HFI) and Sliding Mode Observer (SMO) under the Field-Oriented Control (FOC) framework: the HFI method is employed to extract rotor position information during zero and low-speed stages, while the system switches to the robust SMO for observation during medium and high-speed stages. Secondly, to address the chattering issue commonly occurring at the switching instant between the two algorithms, a smooth weight switching algorithm based on a cubic S-curve is designed. Matlab/Simulink simulation results demonstrate that the proposed scheme not only ensures stable motor operation across the full-speed range but also reduces the peak angular error of chattering by approximately 50% compared to non-switching algorithms, verifying the effectiveness and superiority of the proposed composite rotor position observation method in full-speed range sensorless control.

KEYWORDS

Sensorless Brushless DC Motor; Field-Oriented Control (FOC); High-Frequency Injection (HFI); Sliding Mode Observer (SMO); Switching Algorithm; Simulation Verification.

1. INTRODUCTION

With the rapid development of robotics, aerospace, and industrial automation technologies, Brushless Direct Current (BLDC) motors have become core components of drive systems due to their advantages such as high power density, long life, and high reliability [1]. To reduce the volume of the motor drive system and enhance its reliability in harsh environments, sensorless control technology based on the Field-Oriented Control (FOC) framework has become a focus of research in both academia and industry [2]. In research on the full-speed range operation of BLDC motors, observation strategies are typically divided into two stages based on speed characteristics: in the zero and low-speed stage, saliency-based observation methods are primarily adopted within the industry, with High-Frequency Injection (HFI) being the most representative [3]. This method utilizes rotor saliency to extract position information and does not rely on back electromotive force (EMF), thus solving the difficulties of motor starting and low-speed operation. However, continuous signal injection introduces significant electromagnetic noise and increases high-frequency losses in the system; in the medium and high-speed stage, researchers generally employ model-based methods, such as the Sliding Mode Observer (SMO) [4], which is characterized by algorithmic simplicity and strong robustness, but in the low-speed stage, the observation accuracy of methods like SMO decreases significantly because the back EMF amplitude is close to zero. To address the issue where

a single algorithm cannot cover the full-speed range, this paper constructs a composite rotor position observation method based on HFI and SMO, employing HFI in the low-speed range and switching to SMO in the medium and high-speed range to achieve smooth coverage from standstill to rated speed. However, during the switching process between the two algorithms, the discontinuity of the estimated rotor position values can easily trigger system chattering, affecting the smoothness of motor operation. To resolve these issues, this paper proposes a smooth weight switching algorithm based on a cubic S-curve function to reduce the angle estimation chattering caused at the switching instant. The proposed method is verified through Matlab/Simulink simulations, and the results indicate that the method can achieve stable sensorless control of the BLDC motor across the full-speed range and effectively suppress system shocks during the switching process.

2. FOC FRAMEWORK AND MATHEMATICAL MODEL OF THE MOTOR

This chapter mainly introduces the mathematical model of the Brushless Direct Current (BLDC) motor and the basic architecture of Field-Oriented Control (FOC). This serves as the foundation for subsequent research on the full-speed range composite observer and the smooth switching algorithm.

2.1. Overall Control Strategy of the System

The FOC control system based on the composite observer, constructed in the Matlab/Simulink simulation environment in this paper, is structured as shown in Fig. 1:

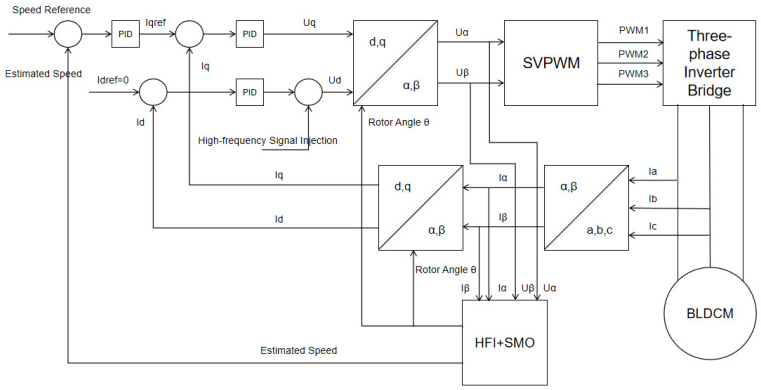

Figure 1. FOC Overall Block Diagram

The parameters of the motor selected for simulation are: the number of pole pairs is 4, the stator resistance is 0.12 Ω, the rated supply voltage is 24 V, the flux linkage is 0.035 Wb, the d-axis inductance is 5.25 mH, and the q-axis inductance is 12 mH.

2.2. Fundamentals of Coordinate Transformation

In order to achieve effective control of the stator currents, coordinate transformations are required. First, the currents in the three-phase stationary coordinate system (abc) are converted into the currents in the two-phase stationary coordinate system (αβ) through the Clarke transformation [5]:

$$\begin{cases} i_\alpha = i_a - \cos\left(\frac{2}{3}\pi\right) i_b - \cos\left(\frac{2}{3}\pi\right) i_c \\ i_\beta = \sin\left(\frac{2}{3}\pi\right) i_b - \sin\left(\frac{2}{3}\pi\right) i_c \end{cases}. \quad (1)$$

Subsequently, the currents are projected onto the rotor synchronous rotating coordinate system (dq) using the Park transformation:

$$\begin{cases} i_d = i_\alpha \cos\theta + i_\beta \sin\theta \\ i_q = -i_\alpha \sin\theta + i_\beta \cos\theta \end{cases}. \tag{2}$$

Ia, ib, ic are the three-phase current values of the brushless motor collected by sensors, which are orthogonalized into the complex plane α-β coordinate system through the Clarke transformation to reduce computational complexity; id and iq represent the motor flux and motor torque components, respectively.

2.3. Mathematical Model of the BLDC Motor

2.3.1. Physical Model in the Three-Phase Stationary Coordinate System

In the ideal state, the three-phase voltage equations of the Brushless Direct Current (BLDC) motor form the foundation of all research [6]. According to the law of electromagnetic induction, the voltage balance equation for each phase can be expressed as the sum of the stator resistance voltage drop, the inductance voltage drop, and the back electromotive force (EMF):

$$\begin{bmatrix} u_a \\ u_b \\ u_c \end{bmatrix} = \begin{bmatrix} R_s & 0 & 0 \\ 0 & R_s & 0 \\ 0 & 0 & R_s \end{bmatrix} \begin{bmatrix} i_a \\ i_b \\ i_c \end{bmatrix} + \begin{bmatrix} L\text{-}M & 0 & 0 \\ 0 & L\text{-}M & 0 \\ 0 & 0 & L\text{-}M \end{bmatrix} \frac{d}{dt} \begin{bmatrix} i_a \\ i_b \\ i_c \end{bmatrix} + \begin{bmatrix} e_a \\ e_b \\ e_c \end{bmatrix}, \tag{3}$$

In the formula, RS is the stator phase resistance; L is the stator self-inductance, and M is the mutual inductance; ea, eb, and ec are the back EMFs of the three phases, respectively.

2.3.2. Mathematical Model in the Two-Phase Stationary Coordinate System

To facilitate the design of the Sliding Mode Observer (SMO), the model is typically projected onto the αβ-axes using the Clarke transformation, and its voltage equations should be rewritten in the extended back EMF form:

$$\begin{cases} u_\alpha = R_s i_\alpha + L_d \frac{d}{dt} i_\alpha + \omega_e (L_d - L_q) i_\beta + e_\alpha \\ u_\beta = R_s i_\beta + L_d \frac{d}{dt} i_\beta - \omega_e (L_d - L_q) i_\alpha + e_\beta \end{cases}, \tag{4}$$

Where eα and eβ are the extended back EMF components containing rotor position information. To construct the current state observer subsequently, Eq. 4 is rearranged into a form with current derivatives as state variables:

$$\begin{cases} \frac{d}{dt} i_\alpha = -\frac{R_s}{L_d} i_\alpha - \frac{\omega_e (L_d - L_q)}{L_d} i_\beta + \frac{1}{L_d} u_\alpha - \frac{1}{L_d} e_\alpha \\ \frac{d}{dt} i_\beta = \frac{\omega_e (L_d - L_q)}{L_d} i_\alpha - \frac{R_s}{L_d} i_\beta + \frac{1}{L_d} u_\beta - \frac{1}{L_d} e_\beta \end{cases}. \tag{5}$$

2.3.3. Analysis of Motor High-Frequency Impedance Characteristics

For the High-Frequency Signal Injection (HFI) method used in the low-speed stage, the motor exhibits significant high-frequency impedance characteristics. Since the frequency of the injected signal is much higher than the fundamental frequency of the motor, the voltage drop across the stator resistance and the back EMF terms can be neglected [7]. At this point, the high-frequency voltage response equations in the rotating dq coordinate system can be simplified as:

This model serves as the theoretical basis for subsequent position extraction utilizing the magnetic saliency of the inductance.

$$\begin{bmatrix} u_{dh} \\ u_{qh} \end{bmatrix} \approx \begin{bmatrix} L_d & 0 \\ 0 & L_q \end{bmatrix} \frac{d}{dt} \begin{bmatrix} i_{dh} \\ i_{qh} \end{bmatrix}, \tag{6}$$

3. DESIGN OF THE COMPOSITE POSITION OBSERVER

3.1. Low-Speed Position Observation Based on Pulsating High-Frequency Voltage Injection (HFI)

3.1.1. High-Frequency Mathematical Foundation Model

When the motor is operating at low speeds or in a stationary state, the back EMF is extremely small, and the Sliding Mode Observer (SMO) cannot effectively extract rotor position information. At this point, a high-frequency voltage signal is injected into the stator windings. Since the signal frequency is much higher than the fundamental frequency, the stator resistance voltage drops and the rotational back EMF terms can be neglected. Consequently, the high-frequency voltage equations in the rotor synchronous rotating dq coordinate system are simplified as:

$$\begin{bmatrix} u_{dh} \\ u_{qh} \end{bmatrix} \approx \begin{bmatrix} pL_d & 0 \\ 0 & pL_q \end{bmatrix} \begin{bmatrix} i_{dh} \\ i_{qh} \end{bmatrix}. \tag{7}$$

In the formula, p is the differential operator. As shown by the above equation, the motor is equivalent to a purely inductive load under high-frequency excitation.

3.1.2. Square-Wave Voltage Injection and Coordinate System Transformation

This paper adopts a square-wave voltage injection scheme based on the estimated rotating coordinate system ($\hat{d}$-$\hat{q}$). Defining the actual rotor position angle as θ and the estimated position angle as $\hat{\theta}$, the position error between the two is $\tilde{\theta} = \theta - \hat{\theta}$.

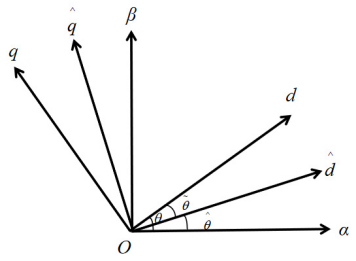

Figure 2. Schematic of the rotor coordinate system

In the figure, α-β is the stationary coordinate system, $\hat{d}$-$\hat{q}$ is the estimated rotating coordinate system, and d-q is the actual rotating coordinate system. Pulsating high-frequency injection involves injecting an estimated high-frequency voltage signal into the $\hat{d}$-$\hat{q}$-axis, where the injected voltage on the estimated $\hat{q}$-axis is zero:

$$\begin{cases} \hat{u}_{dh} = U_{in} sgn(\cos \omega_{in} t) \\ \hat{u}_{qh} = 0 \end{cases}, \tag{8}$$

In the formula, Uin is the amplitude of the injected voltage and ωin is the injection frequency. Through coordinate transformation, the current response equations in the estimated coordinate system can be derived as:

$$\begin{bmatrix} p\hat{i}_d \\ p\hat{i}_q \end{bmatrix} = \frac{1}{L^2-\Delta L^2} \begin{bmatrix} L+\Delta L\cos 2\tilde{\theta} & \Delta L\sin 2\tilde{\theta} \\ \Delta L\sin 2\theta & L-\Delta L\cos 2\tilde{\theta} \end{bmatrix} \begin{bmatrix} \hat{u}_{dh} \\ \hat{u}_{qh} \end{bmatrix}. \tag{9}$$

In the formula, L=(Ld + Lq)/2 represents the average inductance, and ΔL=(Ld — Lq)/2 represents the half-difference inductance.

3.1.3. Rotor Position Error Extraction

Substituting Eq. 8 into Eq. 9 and integrating over one injection period, the integral expression for the high-frequency current response can be obtained:

$$\begin{cases} \hat{i}_d = \frac{U_{in}(L+\Delta L\cos 2\tilde{\theta})}{L^2-\Delta L^2}\int_0^T sgn(\cos\omega_{in}t)dt \\ \hat{i}_q = \frac{U_{in}(\Delta L\sin 2\tilde{\theta})}{L^2-\Delta L^2}\int_0^T sgn(\cos\omega_{in}t)dt \end{cases}. \tag{10}$$

As can be seen from Eq. 10, the estimated quadrature-axis (q-axis) current $\hat{i}_q$ contains the angular error signal $\sin 2\tilde{\theta}$. When the error angle $\tilde{\theta}$ approaches 0, $\hat{i}_q$ also tends toward 0. Therefore, by designing an appropriate filter to extract the envelope signal of $\hat{i}_q$ and processing it through a Phase-Locked Loop (PLL), real-time tracking of the rotor position angle θ can be achieved.

3.2. Medium-to-High Speed Position Observation Based on Sliding Mode Observer (SMO)

In the medium-to-high speed operation phase of the motor, the back EMF amplitude is relatively large, making it suitable to employ a Sliding Mode Observer (SMO) for position estimation. This method offers advantages such as low sensitivity to parameter variations and strong robustness [8].

3.2.1. Coordinate System Selection and Mathematical Model

To simplify calculations and directly extract the back EMF, the SMO is constructed in the two-phase stationary coordinate system (α-β). The current state equations of the motor can be expressed as:

$$p\begin{bmatrix} i_\alpha \\ i_\beta \end{bmatrix} = \begin{bmatrix} -\frac{R_s}{L_d} & -\frac{\omega_e(L_d-L_q)}{L_d} \\ \frac{\omega_e(L_d-L_q)}{L_d} & -\frac{R_s}{L_d} \end{bmatrix} \begin{bmatrix} i_\alpha \\ i_\beta \end{bmatrix} + \frac{1}{L_d}\begin{bmatrix} u_\alpha - E_\alpha \\ u_\beta - E_\beta \end{bmatrix}. \tag{11}$$

In the formula, E_α and E_β are the back-EMF components on the stator α-β axes, which contain the rotor position information. They are defined as:

$$\begin{bmatrix} E_\alpha \\ E_\beta \end{bmatrix} = [(L_d-L_q)(\omega_e i_d - p i_q) + \psi_f\omega_e] \begin{bmatrix} -\sin\theta_e \\ \cos\theta_e \end{bmatrix}. \tag{12}$$

3.2.2. Sliding Mode Observer Design and Control Law

$$p\begin{bmatrix} \hat{i}_\alpha \\ \hat{i}_\beta \end{bmatrix} = \begin{bmatrix} -\frac{R_s}{L_d} & -\frac{\omega_e(L_d-L_q)}{L_d} \\ \frac{\omega_e(L_d-L_q)}{L_d} & -\frac{R_s}{L_d} \end{bmatrix} \begin{bmatrix} \hat{i}_\alpha \\ \hat{i}_\beta \end{bmatrix} + \frac{1}{L_d}\begin{bmatrix} u_\alpha - v_\alpha \\ u_\beta - v_\beta \end{bmatrix}. \tag{13}$$

Based on the physical model mentioned above, the current observer is constructed as in formula (13). Where $\hat{i}_\alpha$, $\hat{i}_\beta$ are the estimated current values; u_α, u_β are the sliding mode control law inputs. To enable the estimated currents to converge rapidly to the actual currents, the sliding surface is defined as the current observation error $s = \hat{i} - i = 0$. The following sliding mode control law is constructed using the sign function (sgn):

$$\begin{bmatrix} v_\alpha \\ v_\beta \end{bmatrix} = \begin{bmatrix} z \cdot sgn(\hat{i}_\alpha - i_\alpha) \\ z \cdot sgn(\hat{i}_\beta - i_\beta) \end{bmatrix}. \tag{14}$$

In the formula, z is the sliding mode gain, and its value must satisfy the Lyapunov stability criterion to ensure that the system enters the sliding mode state within a finite time.

3.2.3. Stability Analysis and Position Extraction

Subtracting Eq. 11 from Eq. 13, the current observation error equation can be obtained:

$$p\begin{bmatrix} i_\alpha^* \\ i_\beta^* \end{bmatrix} = \begin{bmatrix} -\frac{R_s}{L_d} & -\frac{\omega_e(L_d - L_q)}{L_d} \\ \frac{\omega_e(L_d - L_q)}{L_d} & -\frac{R_s}{L_d} \end{bmatrix} \begin{bmatrix} i_\alpha^* \\ i_\beta^* \end{bmatrix} + \frac{1}{L_d} \begin{bmatrix} E_\alpha - v_\alpha \\ E_\beta - v_\beta \end{bmatrix}. \tag{15}$$

In the formula, $i_\alpha^* = \hat{i}_\alpha - i_\alpha$ is the current error. When the system enters the sliding mode state, it satisfies $i_\alpha^* = i_\beta^* = 0$ and their derivatives are 0. At this point, the sliding mode control variables v_α, v_β are equivalent to the back-EMF components E_α, E_β. Since v is a switching signal containing high-frequency chattering, it is necessary to filter out the high-frequency switching noise in v_α, v_β through a low-pass filter (LPF) to obtain smooth back-EMF estimated values E_α, E_β.

$$\begin{cases} E_\alpha = \frac{\omega_c}{p + \omega_c} v_\alpha \\ E_\beta = \frac{\omega_c}{p + \omega_c} v_\beta \end{cases}. \tag{16}$$

In the formula, ω_c is the cutoff frequency. Finally, the obtained back-EMF estimated values are input into a Phase-Locked Loop (PLL). By using a PI regulator to track the direction of the back-EMF vector in a closed loop, real-time and accurate extraction of the rotor position angle θe and rotational speed ω_e can be achieved.

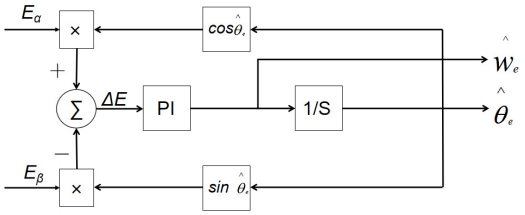

Figure 3. Flowchart of the PLL algorithm

The smooth back-EMF obtained from Eq. 16 serves as the input signal for the phase-locked loop (PLL).

3.3. Design of Observer Switching Algorithm for Full Speed Range

3.3.1. Necessity of the Switching Algorithm

In brushless DC motor (BLDC) sensorless control systems, a single observer is difficult to cover the full speed range. The high-frequency pulsating injection (HFI) method exhibits excellent observation performance at zero and low speeds; however, as the speed increases, the injected high-frequency voltage signals introduce additional electromagnetic losses and high-frequency noise, and are highly susceptible to interference from the nonlinear characteristics of the inverter. In contrast, the sliding mode observer (SMO) relies on the extraction of back-EMF components E_α and E_β. Since the back-EMF amplitude of a BLDC is proportional to the speed, the back-EMF signal is extremely weak during low-speed operation, making it difficult for the SMO to guarantee observation accuracy or even causing it to fail. Therefore, to leverage the respective advantages of both algorithms, this paper proposes incorporating the HFI algorithm into the SMO framework. However, there is often a certain angular observation deviation $\Delta\theta$ at the instant of switching between the two. If a direct switching method is used, the abrupt change in angle will directly lead to severe fluctuations in the stator current I_q. This current surge can trigger significant torque ripple and mechanical vibration, and in severe cases, even lead to motor startup failure or loss of synchronism. Consequently, to bridge the "control blind zone" between the two algorithms, this paper proposes introducing HFI into the SMO framework to form a composite observer and designing a smooth transition algorithm to ensure the continuity of rotor position estimation during the switching process.

3.3.2. Smooth Weight Switching Algorithm Based on Cubic S-type Function

To ensure the continuity of the switching process, this paper adopts a weighted fusion strategy based on a cubic polynomial interpolation function. By constructing an S-shaped weighting factor M , the algorithm dynamically allocates the weights of HFI and SMO within the transition interval. The values of the weighting coefficients are shown in Fig. 3:

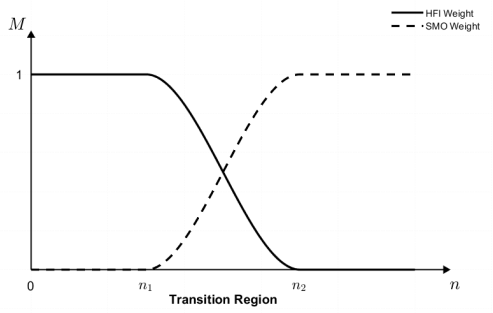

Figure 4. Weighting factor function curve

Set the lower switching speed limit as n_{low} and the upper limit as n_{high}. Define the normalized speed change rate ratio as:

$$ratio=\frac{\hat{n}-n_{low}}{n_{high}-n_{low}}. \tag{17}$$

Introduce the cubic interpolation weighting factor M, whose mathematical model is:

$$M=\begin{cases}1, & \hat{n}\le n_{low}\\ 1-3\cdot ratio^2+2\cdot ratio^3, & n_{low}<\hat{n}<n_{high}.\\ 0, & \hat{n}\ge n_{high}\end{cases} \tag{18}$$

The estimation results of the two observers are dynamically allocated in real time by a weighting factor M, yielding the final estimated speed $\hat{n}$ and the estimated electrical angle $\hat{\theta}_e$ of the system.

$$\begin{aligned} \hat{n} &= M \cdot \hat{n}_{HFI} + (1-M) \cdot \hat{n}_{SMO} \\ \hat{\theta}_e &= M \cdot \hat{\theta}_{HFI} + (1-M) \cdot \hat{\theta}_{SMO} \end{aligned} \quad (19)$$

Under this strategy, when the motor starts from zero speed, the system operates entirely in the HFI mode. As the speed increases and enters the transition region, the weighting factor M decreases smoothly according to an S-shaped curve, such that the contribution of the SMO gradually increases. Once the speed exceeds n_{high}, the system is completely switched to the SMO mode.

4. MATLAB SIMULATION VERIFICATION AND RESULTS ANALYSIS

4.1. Overall Structure and Parameter Settings of the Simulation System

An FOC control system was established within the MATLAB/Simulink environment. All subsequent tests were conducted under a constant load torque of 2 N·m. The reference speed profile was set to ramp from 0 to 300 r/min between 0 and 0.2 s, remaining stable from 0.2 to 1 s. Subsequently, the speed increased to 1000 r/min from 1 to 2 s and maintained stability thereafter. The overall block diagram of the sensorless control system for the full speed range is shown in Fig. 5.

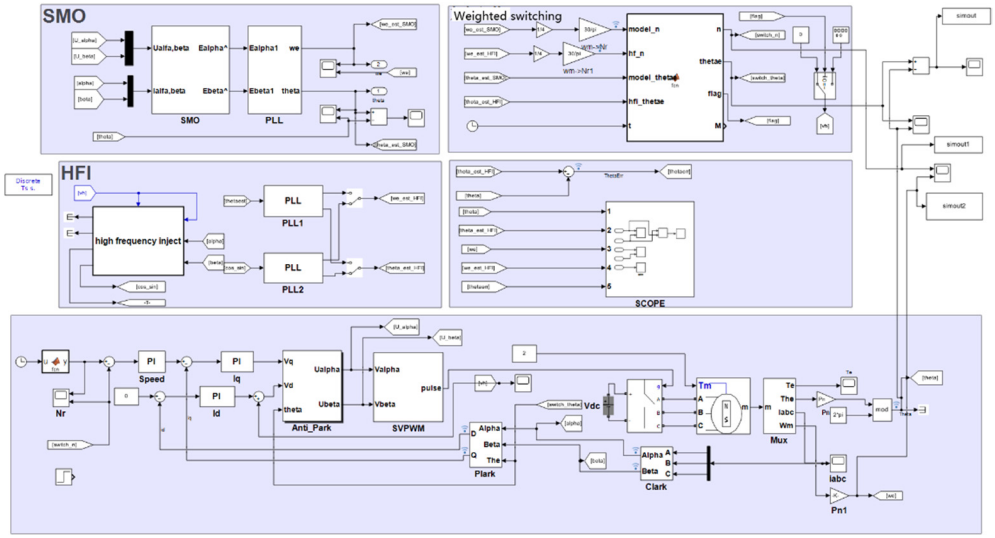

Figure 5. Overall block diagram of the full-speed range sensorless control system

4.2. Performance Analysis of Pulsating High-Frequency Injection (HFI)

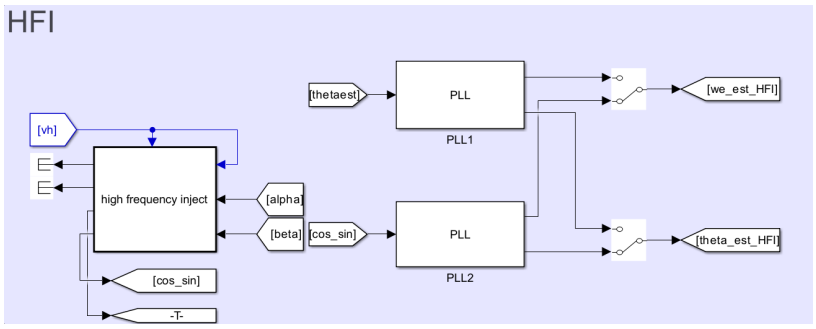

Figure 6. HFI rotor position estimation module

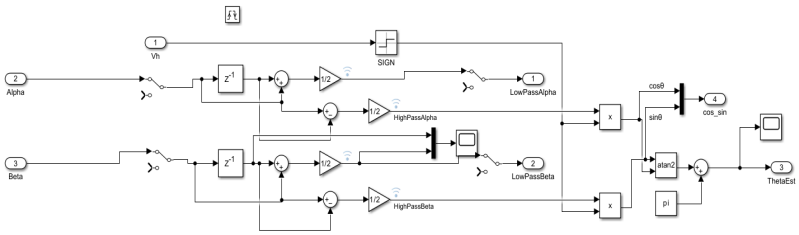

Figure 7. HFI High-frequency Response Signal Demodulation Module

The core of the position observation module in this system consists of an HFI-based rotor position estimation unit and an internal high-frequency response demodulation module. The high-frequency current component is extracted through a z^{-1} block, then demodulated by a multiplier and processed by an atan2 function to obtain the position error, and finally fed into a phase-locked loop (PLL) to output the real-time speed and rotor angle. This structure provides accurate low-speed feedback for the system, and the corresponding observation results are shown as follows:

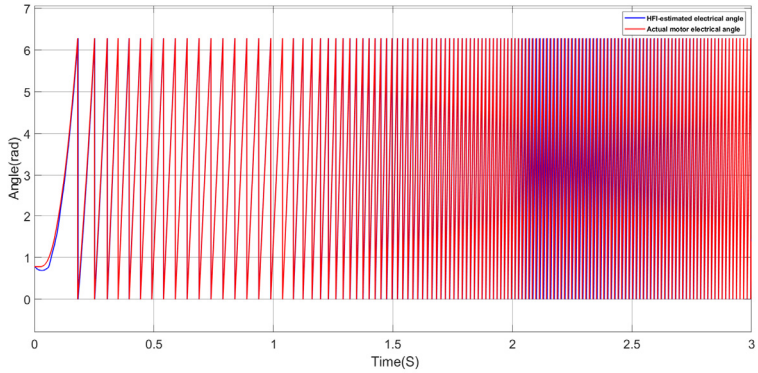

Figure 8. Comparison between HFI-estimated electrical angle and actual electrical angle

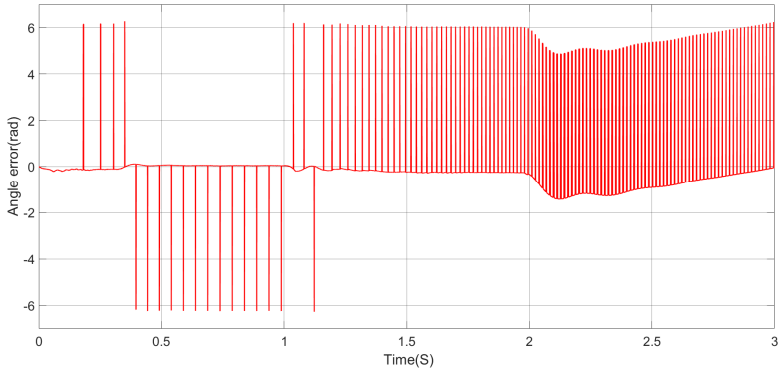

Figure 9. Error curve of HFI-estimated electrical angle

As shown in Fig. 8 and Fig. 9, during motor startup and low-speed operation (n<300r/min), the electrical angle estimated by the HFI method is almost identical to the actual rotor angle. When the speed increases to 1000 r/min, the observation performance of HFI deteriorates. As illustrated in Fig. 8, the estimated angle waveform begins to deviate from the actual angle, while Fig. 9 indicates that the angle error not only fluctuates severely but also exhibits a significant bias. This degradation is mainly caused by the enhancement of the motor back-EMF at high speeds, whose harmonic components overlap with the injected high-frequency carrier, making it difficult for the demodulation module to accurately extract the position error signal. In addition, the increase in high-frequency impedance with speed leads to a reduced signal-to-noise ratio, rendering the HFI algorithm unsuitable for medium- and high-speed operating conditions.

4.3. Performance Analysis of the Sliding Mode Observer (SMO)

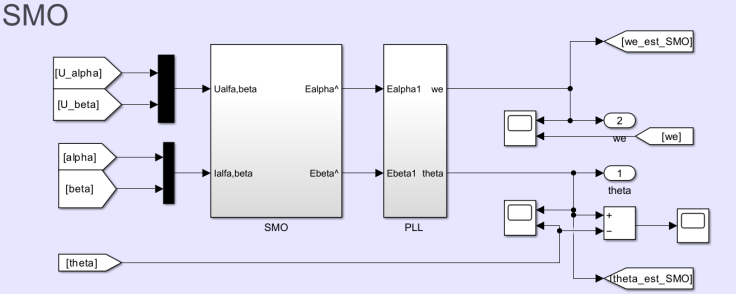

Figure 10. SMO-based rotor position estimation module

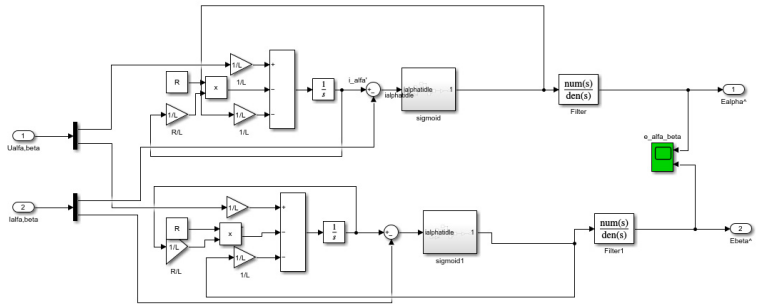

Figure 11. SMO-based back-EMF estimation module

The medium- and high-speed observation scheme of the system is illustrated in Fig. 10 and Fig. 11. The SMO-based position estimation module receives the voltage and current signals, estimates the back-EMF through the internal sliding mode observer, and employs a phase-locked loop (PLL) to obtain the real-time electrical speed ω_e and electrical angle θe. The back-EMF estimation module is implemented within the SMO block. By combining a current observer with a sigmoid continuous control function, the chattering of the sliding mode is effectively suppressed, and smooth back-EMF components E_α and E_β are extracted using a low-pass filter, providing high signal-to-noise ratio signals for angle calculation. The corresponding observation results are presented as follows:

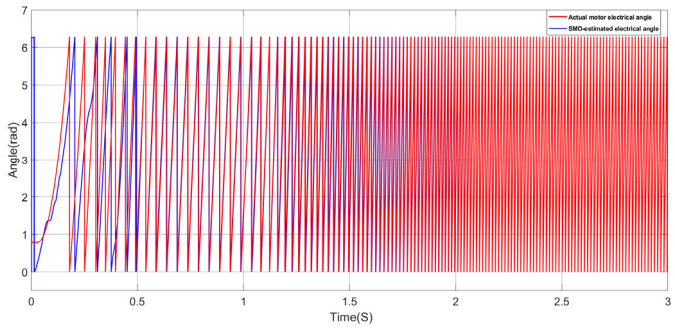

Figure 12. Comparison between SMO-estimated electrical angle and actual electrical angle

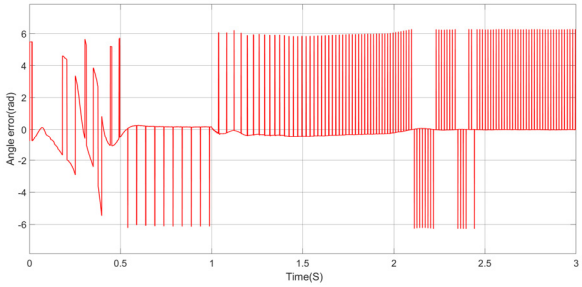

Figure 13. Error curve of SMO-estimated electrical angle

As shown in Fig. 12 and Fig. 13, during motor startup and low-speed operation, the estimated angle waveform exhibits a significant phase lag relative to the actual rotor angle, and the angle error fluctuates severely, indicating that the SMO is inadequate for zero- and low-speed conditions. As the motor speed increases to 300 r/min and then to 1000 r/min, the estimated angle can rapidly lock onto and accurately track the actual rotor position, with the angle error converging near 0 rad and exhibiting minimal fluctuation and no evident bias. This performance is attributed to the sliding mode observer, which, based on the current state equations, can accurately extract the back-EMF components from the strong electromagnetic signals at high speeds. Coupled with the chattering suppression effect of the sigmoid function, the system demonstrates excellent robustness and steady-state observation accuracy in the medium- and high-speed range.

4.4. Performance Analysis of the HFI–SMO Hybrid Approach

As shown in Fig. 5, based on the previously analyzed speed-domain characteristics of HFI and SMO, this section presents the combined observation performance of the system over the full speed range. During zero- and low-speed operation ($0 < t < 1s$), the system utilizes the estimated angle provided by the HFI module. When the motor speed enters the medium- and high-speed range ($t > 1s$), the system switches to the observation output of the SMO module.

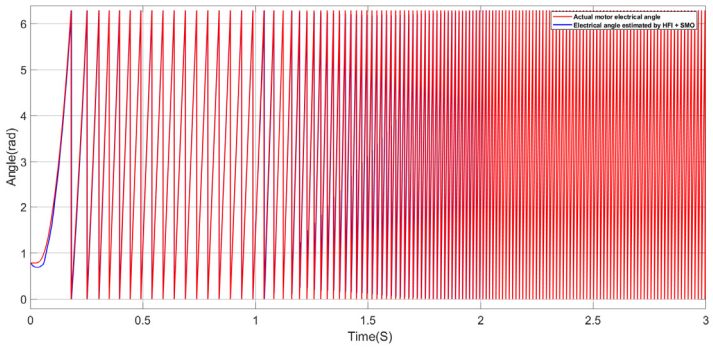

Figure 14. Comparison between HFI+SMO-estimated electrical angle and actual electrical angle

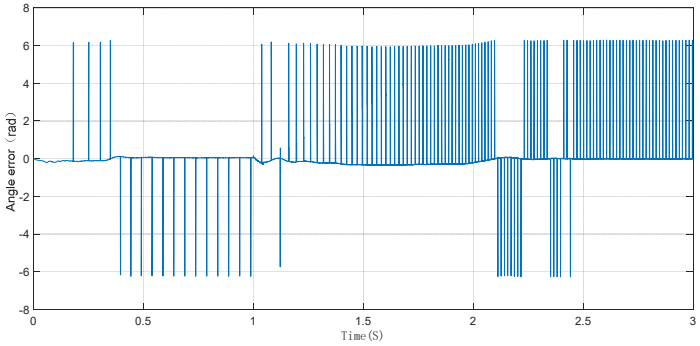

Figure 15. Error curve of HFI+SMO-estimated electrical angle

As shown in Fig. 14 and Fig. 15, the combined observation scheme solves the problem that a single observer cannot cover the full speed range. Throughout the entire speed regulation range, the estimated speed closely tracks the reference speed, and the position error remains within the allowable range, verifying the feasibility of using the high-frequency injection (HFI) method at low speeds and the sliding mode observer (SMO) at high speeds.

However, a closer examination of the error curve in Fig. 15 reveals that at 1 s, when the speed reaches 300 r/min, the system exhibits noticeable transient chattering and current spikes. In view of this, to eliminate the negative effects caused by direct switching and achieve seamless transitions between observers in the transition region, a weighted smooth switching algorithm based on a cubic S-shaped function is introduced, which will be presented in the following section.

4.5. Implementation of the Smooth Switching Algorithm for the Sensorless Hybrid Observation System

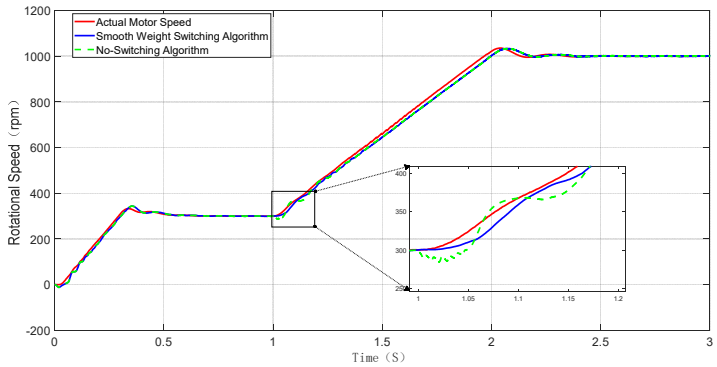

Figure 16. Comparison of Rotational Speed Between Smooth Weight Switching and No-Switching Algorithms

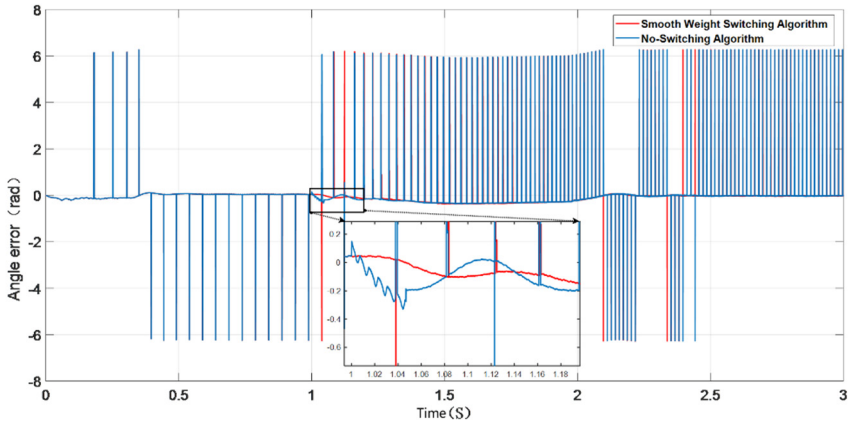

Figure 17. Comparison of Angular Error Between Smooth Weight Switching and No-Switching Algorithms

In the simulation, the motor speed rises from 0 to 300 r/min within 0–0.2 s and remains stable from 0.2–1 s. It then increases to 1000 r/min during 1–2 s and maintains stable operation after 2 s. When the motor speed is below 300 r/min, the rotor position is observed using the high-frequency injection (HFI) method. When the speed exceeds 300 r/min, the system enters the switching stage of the HFI and sliding mode observer (SMO) hybrid observation. After the speed exceeds 400 r/min, the rotor position is fully observed by the SMO.

As shown in Fig. 16, at 1.0 s (speed of 300 r/min), the system enters the HFI–SMO switching region. Without a switching algorithm, noticeable oscillations appear around 1.04 s, and the speed drops to 280 r/min, indicating that the abrupt change of the observer output during hard switching imposes a significant impact on the speed loop. In contrast, with the switching algorithm, the transition process is very smooth, without obvious overshoot or drop. This verifies that the cubic S-shaped weighting function achieves a smooth transition of the weights, and the motor fluctuations with the smooth weighted switching algorithm are smaller than those without switching.

Fig. 17 shows the comparison of angle errors. At the switching instant of 1.0 s, the angle error exhibits significant high-frequency chattering, with a maximum fluctuation range close to 0.4 rad, and the waveform is irregular. In the same interval, the curve using the smooth switching algorithm is much smoother, with error fluctuations limited within 0.2 rad, reducing the peak error by approximately 50% compared to the no-switching case.

In summary, the cubic S-shaped smooth weighted switching algorithm effectively suppresses motor chattering, demonstrating its superiority in mitigating system switching shocks and improving operational quality across the full speed range.

5. SUMMARY

Addressing the challenge of full-speed range sensorless control for Brushless DC Motors (BLDC), this paper researches and designs a composite position observation system combining HFI and SMO, based on the establishment of the FOC framework and the motor's mathematical model. By employing the pulsating High-Frequency voltage Injection (HFI) method during the low-speed stage, position tracking at zero and low speeds is achieved by utilizing rotor saliency characteristics. In the medium-to-high speed range, a Sliding Mode Observer (SMO) is utilized to ensure operational robustness based on the back-EMF principle. To mitigate the chattering issues occurring in the transition zone between the two algorithms, this paper proposes a smooth switching algorithm based on a cubic S-type function, which achieves a nonlinear and continuous weight transition within the switching interval. Matlab simulation results demonstrate that the proposed composite observation scheme eliminates the speed and angle impulses caused by traditional hard switching, achieving stable operation and seamless position observation throughout the entire process from standstill startup to rated speed. This validates the effectiveness and practical engineering value of the proposed strategy.

REFERENCES

[1] Akrami M, Jamshidpour E, Nahid-Mobarakeh B, et al. Sensorless control methods for BLDC motor drives: A review[J]. IEEE Transactions on Transportation Electrification, 2024, 11(1): 135-152. https://doi.org/ 10. 1016/ j. compositesb.2016.10.015.

[2] Li N, Li M, Zhang C, et al. Design of brushless motor control system based on FOC algorithm[C]//International Conference on Mechatronic Engineering and Artificial Intelligence (MEAI 2023). SPIE, 2024, 13071: 672-678. https://doi.org/10.1117/12.3025713.

[3] Bahrami-Fard M, Korrani M G, Fahimi B. Sensorless Field Oriented Control of CSI-Fed PMSM Drives Used in Submersible Pumps[J]. arXiv preprint arXiv:2503.22855, 2025. https://doi.org/10.48550/arXiv.2503.22855.

[4] Sohel R M, Wu W, Ji R, et al. Sliding Mode Observer-Based Sensorless Control Strategy for PMSM Drives in Air Compressor Applications[J]. Applied Sciences, 2025, 15(20): 11206. https://doi.org/10.3390/app152011206.

[5] Chattopadhyay S, Mitra M, Sengupta S. Clarke and park transform[M]//Electric Power Quality. Dordrecht: Springer Netherlands, 2011: 89-96. https://doi.org/10.1007/978-94-007-0635-4_12.

[6] Agarwal N K, Kumar R, Yadav H, et al. Mathematical Modeling and Speed Control of Brushless DC (BLDC) Motor using PID Controllers for the Systems Sustainability[C]//2024 1st International Conference on Sustainability and Technological Advancements in Engineering Domain (SUSTAINED). IEEE, 2024: 143-148. https://doi.org/ 10. 1109/SUSTAINED63638.2024.11074008.

[7] Lee S, Lee W, Liu M, et al. High-frequency motor impedance analysis and CM current estimation of electric motors with concentrated and toroidal windings[J]. IEEE Transactions on Transportation Electrification, 2024, 11(1): 880-890. https://doi.org/10.1109/TTE.2024.3397713.

[8] Kumar S, Singh B. Sensorless Super-Twisting SMO Based PMSM Drive with Improved DANF-PLL for Hybrid Three-Wheeler EV Application[J]. IEEE Transactions on Industry Applications, 2025. https://doi.org/ 10. 1109/ TIA.2025.3567433.